

Epitaxial Growth of Iron Phthalocyanine at the Initial Stage on Au(111) Surface

Z. H. Cheng, L. Gao, Z. T. Deng, Q. Liu, N. Jiang, X. Lin, X. B. He, S. X. Du, and H.-J. Gao*

Beijing National Laboratory for Condensed Matter Physics, Institute of Physics, Chinese Academy of Sciences, P.O. Box 603, Beijing 100080, China

Received: September 18, 2006; In Final Form: December 15, 2006

Growth behavior of iron(II) phthalocyanine (FePc) molecules on Au(111) surface at the initial stage is studied with low-temperature scanning tunneling microscopy. The FePc molecules are separately adsorbed on the face-centered cubic and the hexagonal close-packed regions at the submonolayer regime, indicating that the molecular adsorption is greatly affected by the molecule–substrate interaction. At the monolayer regime, the molecules can form a close-packed ordered structure. When the FePc goes further to the second layer, the unit cell of the formed molecular superstructure shifts compared with the unit cell of the first layer. Comparison of the growth behavior between the FePc and the CoPc also is made to understand the growth difference within the family of the phthalocyanine (Pc) molecules. And it is found that the central metal atom of the metal Pc makes a main contribution to the shift. Our results are helpful for understanding the growth of the Pc molecule family and controlling the related physical properties.

Introduction

Organic semiconductors have attracted considerable interests over the past several decades because of their promising applications in optical and electronic devices, such as organic light-emitting diodes and organic thin-film transistors.^{1,2} Recently, organic molecular thin films on different kinds of substrates have become increasingly important in both the theoretical aspects and the potential application in molecular nanoelectronic devices.^{3–6} Therefore, the initial growth and adsorption behavior on metallic surfaces have been intensively reported.^{7–19} Among functional organic compounds, phthalocyanines (Pcs), metal phthalocyanines (MPcs), and their derivatives have attracted special interest of researchers because of their wide applications in the area of gas-sensing devices, photovoltaic applications, light-emitting diodes, solar and fuel cells, organic field effect transistors, pigments, and dyes.^{20–22} Recently, a variety of scanning tunneling microscopy (STM) studies on the surface assembly of MPcs have been carried out in ultrahigh-vacuum (UHV), solid/liquid interface, and in air. Hipps' group studied the assembling structure of various MPcs including FePc, NiPc, CoPc, and CuPc on Au(111) by using STM in UHV.^{23–26} Their results show that different central metal atoms result in different contrast because of their different d orbital occupations. Itaya's group succeeded in the preparation of well-defined adlayers of CoPc, CuPc, and ZnPc on the Au(111) surface by immersing an Au(111) substrate into a benzene solution saturated with the molecules by means of electrochemical STM.^{27–29} However, these reported results are mainly focused on the monolayers. To better understand the molecular growth and further control the physical properties, growth information from submonolayer to multilayer is needed.^{30,31}

In this paper, we present the growth process of FePc molecules adsorbed on Au(111) from low coverage of submonolayer, monolayer, to second layer studied with low-temperature STM (LTSTM). The specific adsorption sites at the initial growth stage and the molecular structure of the

ongoing thin film have been systematically investigated. In addition, we compared our results with that of the CoPc for understanding the difference in the growth process, and found that the difference is attributed to the different central metal atom in the MPcs.

Experimental Section

The experiments were performed with a combined UHV molecular beam epitaxy-LTSTM (MBE-LTSTM) system at a base pressure in the range of 10^{-10} mbar. The single-crystal Au(111) substrate (99.999% and orientation accuracy < 0.1 deg) was purchased from MaTecK (Germany). The clean Au(111) surface was prepared by repeated cycles of Ar ion sputtering and annealing at 700 K in the preparation chamber. Then the bare Au(111) surface was scanned to get the atomic resolution STM image for determining the surface orientations. FePc (Aldrich, 98+%) materials were effectively purified using the temperature gradient sublimation method and immediately loaded into the sublimation cells.³² FePc molecules were thermally evaporated at 540 K onto the Au(111) surface kept at variable temperatures with MBE low-energy electron diffraction (LEED).^{18,19} The FePc evaporation rate is about 0.025 mL/min. A monolayer is defined as the amount of deposited FePc that entirely covers the substrate surface. The whole STM was at 5 K, and all the STM measurements were conducted at 5 K. Electrochemically etched poly crystalline tungsten tips were used as STM tips,³³ which were further cleaned by Ar ion sputtering and annealing in UHV. All given voltages are referred to the sample and the images have been taken in constant-current mode.

Results and Discussion

A. FePc Molecule and Au(111) Surface. All MPcs have a similar molecular structure, containing a central metal atom surrounded by a Pc skeleton. They can be classified into planar and nonplanar molecules because of the different ionic radii of the central metal atom. In the case of nonplanar MPc, the central

* Corresponding author. E-mail: hjgao@aphy.iphy.ac.cn.

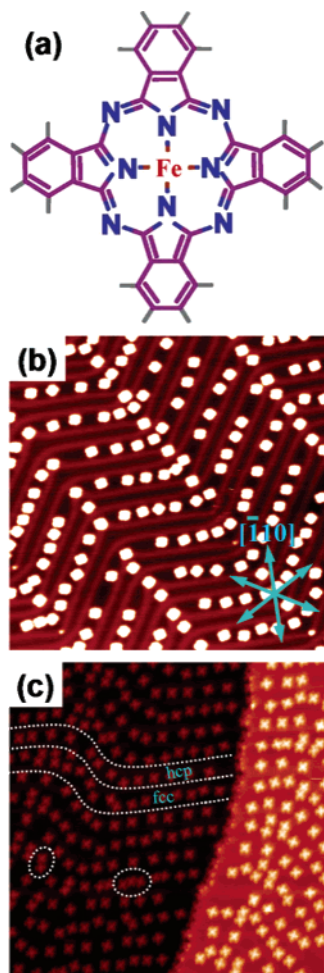


Figure 1. (a) Schematic molecular structure of iron(II) phthalocyanine (FePc). STM images of FePc submonolayer (b) and (c) on Au(111). (b) ~ 0.1 mL ($50 \text{ nm} \times 50 \text{ nm}$, $V = -1.5 \text{ V}$, $I = 0.05 \text{ nA}$); (c) ~ 0.3 mL ($50 \text{ nm} \times 50 \text{ nm}$, $V = -2.0 \text{ V}$, $I = 0.05 \text{ nA}$). The set of three arrows indicates the close-packed directions of the Au(111) substrate. The orientations of all images are identical. Broken white lines indicate domain walls of the Au(111) surface reconstruction. The color scale extends over a range of 0.08 nm in (b) and 0.5 nm in (c).

metal atom is too large to fit completely into the central cavity. Therefore it sticks out of the molecular plane, such as SnPc and PbPc. FePc is a typical planar MPc molecule, which is composed of a flat porphyrin ring bonded to four benzene rings with a single iron ion completely in the central cavity, as schematically shown in Figure 1(a).

Clean Au(111) surface exhibits a well-known $22 \times \sqrt{3}$ herringbone reconstruction, consisting of pairs of periodically bent corrugation lines across terraces and monatomic step edges.³⁴ The slightly elevated surface ridges, which appear as 0.3 \AA protrusions in STM images, correspond to the transitional regions where the topmost layer of the gold atoms are partially dislocated with respect to both face-centered cubic (fcc) and hexagonal close-packed (hcp) hollow sites of the bulk layers. The wider depressions between the ridges are fcc regions where the topmost layer of gold atoms are stacked on top of the second layer fcc hollow sites, whereas the surface gold atoms in the narrower depressions (hcp regions) between ridges are stacked on top of the hcp second layer hollow sites. The 120° bending of the elevated ridge pairs delimits the boundaries between rotational domains of the herringbone reconstruction. The elbows of the Au(111) reconstruction provide the preferential adsorption sites for atoms and molecules.

Understanding the interaction between MPc and metal surface is a critical issue required for controlling the formed structure and its corresponding physical and chemical properties. As for the MPc/Au(111) system, the bonding between the MPc and the Au(111) surface can distinctly affect the charge distribution and the geometric configuration of the molecules at interface. The MPc molecular structure on the Au(111) is mainly determined by the interaction between the central metal atom and the Au(111) substrate.

B. Submonolayer. FePc molecules were thermally evaporated onto the Au(111) surface that was kept at room temperature. At very low coverage, it is found that there is almost no molecules on the large open reconstructed terrace, while on the step edges FePc molecules can be observed in the STM images at 5K, indicating the high mobility of FePc molecules on Au(111) surface. With increasing the molecular coverage, the step edges of the Au(111) are almost fully decorated with molecules. The FePc molecules formed on the terraces of Au(111) shows that the planar skeleton is parallel to the metal surface, exhibiting a four-lobed structure with a protrusion at the center as shown in Figure 1, which is a typical STM image for a planar MPc on metal substrate.

Low Coverage. Figure 1(b) displays a typical STM image of ~ 0.1 mL FePc molecules on Au(111). It can be seen that the FePc molecules are almost completely adsorbed on the fcc regions of the reconstructed Au(111) surface. Meanwhile, there is almost no molecule adsorbed on the hcp regions, whereas only a single molecule can be found at the elbow of the hcp regions. This preferential adsorption behavior indicates that the adsorption of FePc molecule is more stable on fcc than that on the hcp region. The set of the three arrows in Figure 1(b) represent the equivalent close-packed directions of the Au(111) substrate.

High Coverage. At the coverage of ~ 0.3 mL, the FePc molecules adsorbed on both the fcc and the hcp regions of the reconstructed Au(111), as shown in Figure 1(c). Broken white lines represent domain walls of the reconstruction. At this coverage, the molecules on hcp regions distributed dispersedly. In contrast, the molecules on fcc regions are more densely packed than that on hcp regions. It also can be found that there are some dimer-like and trimer-like molecular structures, marked with dashed circles in the STM image mainly distributed at the elbow of the fcc regions. It can also be observed that the step edges are densely decorated with molecules. This is because of the higher adsorption energy on the step edges. And at low coverage, the similar phenomenon also was observed on the step edges.

C. Monolayer. The highly ordered FePc monolayer was fabricated by evaporating FePc onto the Au(111) substrate that was kept at 390 K. Figure 2(a) shows a large scale STM image of a highly ordered FePc monolayer on Au(111). A monolayer is defined as the amount of deposited FePc that entirely covers the substrate surface. A zigzag pattern can be clearly seen as a modulation of the monolayer contrast in the STM image. This zigzag pattern stems from the Au(111) surface reconstruction that provides evidence that the Au(111) surface reconstruction is not destroyed or lifted upon deposition of the FePc molecules at this deposition condition.

An STM image of the FePc monolayer (Figure 2(b)) gives directly the real-space configuration of individual molecules and the periodic structure of the organic monolayer. The observed FePc molecules are recognized as a four-lobed pattern with a protrusion at the center, which is consistent with that observed at submonolayer regime. The orientation of the Au(111) surface

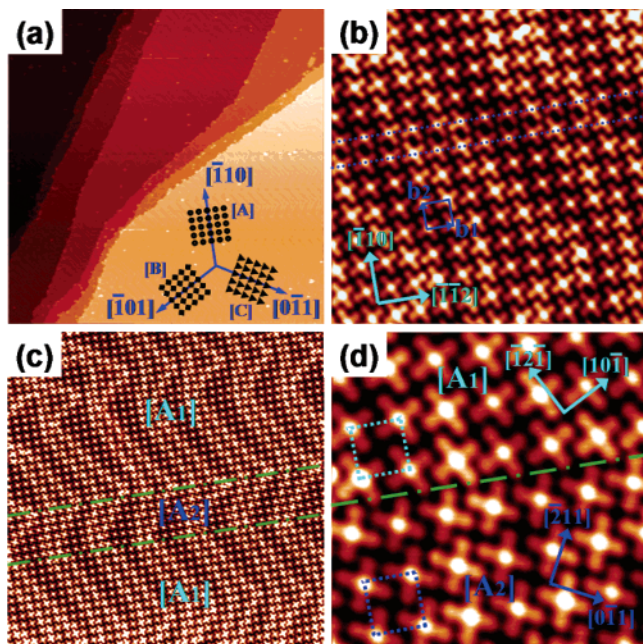


Figure 2. STM images of the first monolayer of FePc on Au(111). (a) 300 nm × 300 nm, $V = -1.2$ V, $I = 0.05$ nA; (b) 20 nm × 20 nm, $V = -0.4$ V, $I = 0.05$ nA. (c) 60 nm × 60 nm, $V = -0.4$ V, $I = 0.05$ nA; (d) 10 nm × 10 nm, $V = -0.4$ V, $I = 0.05$ nA. The inset of (a) shows the sketch of three symmetry-equivalent domains ([A], [B] and [C]) with the underlying Au(111) substrate. One line defect and one unit cell are marked with dashed lines and a square in (b), respectively. Two orientation-domains in the first FePc monolayer on Au(111) are shown in (c). The dashedotted lines indicate the domain boundaries. High-resolution STM image (d) shows the orientations of molecules in both of the orientation-domains. The color scale extends over a range of 2 nm in (a) and 0.08 nm in (b)–(d).

is denoted by thin arrows in the image. A quadratic periodic structure of the FePc monolayer was found in the STM image in which the molecules are aligned one by one along the $[\bar{1}10]$ and $[\bar{1}\bar{1}2]$ directions. A square unit cell is marked by blue lines in which the blue arrows (\mathbf{b}_1 , \mathbf{b}_2) represent the unit cell vectors of the molecular superstructure. On the basis of those STM images, we calculate the relationship between the unit cells of the molecular structure and the substrate, the superstructure matrix. Fourier transformation of several images provides a mean value for the unit cell parameters accounting 15 ± 1 Å and 15 ± 1 Å with an angle of $90 \pm 5^\circ$. LEED measurements (not shown here), show a regular twelve-fold pattern for the first-order spots with six spots along the high-symmetry directions of the substrate. This confirms an angle of 90° for the superstructure unit cell with one side parallel to a high-symmetry direction of the substrate. Therefore, a commensurate superstructure with the following matrix is proposed:

$$\begin{bmatrix} \mathbf{b}_1 \\ \mathbf{b}_2 \end{bmatrix} = \begin{bmatrix} 5 & 0 \\ -3 & 6 \end{bmatrix} \cdot \begin{bmatrix} \mathbf{a}_1 \\ \mathbf{a}_2 \end{bmatrix}$$

Vectors \mathbf{a}_1 and \mathbf{a}_2 are primitive lattice vectors of the Au(111) surface, $\mathbf{a}_1 = \mathbf{a}_2 = 2.86$ Å. Therefore, the lengths of the near quadratic primitive unit cells are $\mathbf{b}_1 = 14.3$ Å and $\mathbf{b}_2 = 14.9$ Å, which agrees well with the experimental results.

Because of the 3-fold symmetry of the Au(111) substrate, three symmetry-equivalent domains of the monolayer are observed in our STM results.^{9,35,36} The inset of Figure 2(a) presents the sketch of the three symmetry-equivalent domains ([A], [B], and [C]) with the underlying Au(111) substrate. Normally, there is only symmetric domain even on a large

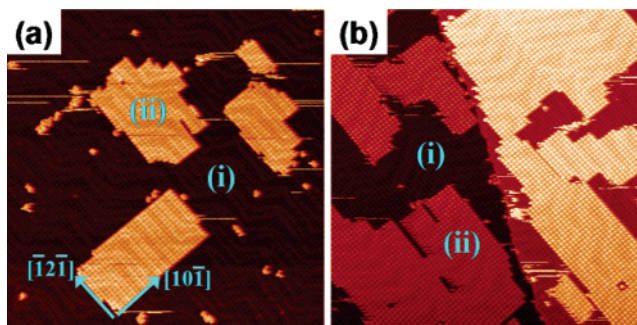


Figure 3. Large-scale STM images of FePc multilayer on Au(111). (a) ~ 1.3 mL (120 nm × 120 nm, $V = -2.2$ V, $I = 0.05$ nA); (b) ~ 1.7 mL (120 nm × 120 nm, $V = -2.2$ V, $I = 0.04$ nA). The growth mode of the second layer is fully different from that of the first layer. The color scale extends over a range of 0.5 nm in (a) and 0.8 nm in (b), respectively.

terrace (i.e., the density of the symmetric domain boundary is rather low in the well-ordered monolayer). It is found that there is a kind of line defect in the ordered monolayer, marked by double dashed lines in Figure 2(b). These line defects make the periodically shifted lattice within two parts of a domain. Figure 2(c) shows a large scale STM image of the [A] domain, which consist of two molecular orientations-domains, [A1] and [A2]. The domain boundaries are indicated by the dashedotted lines in Figure 2(c).

Figure 2(d) represents the orientation-domain boundary and the real-space orientation of individual molecules in both [A1] and [A2] orientation-domains. Two square unit cells in [A1] and [A2], marked by dashed lines, show the same size and lattice orientations, respectively. In contrast, the orientation of the FePc molecules in [A1] and [A2] is different, marked by the arrows. The orientations of FePc molecules in [A1] are along the $[\bar{1}2\bar{1}]$ and $[10\bar{1}]$ directions, and those in [A2] are along the $[\bar{2}11]$ and $[011]$ directions, which are mirrored with respect to the $[\bar{1}\bar{1}2]$ and $[\bar{1}10]$ directions of the Au(111) substrate. Considering the substrate symmetry, we can conclude that the FePc molecules in [A1] and [A2] show the identical adsorption sites. As shown in the STM image, even near the boundaries the ordered arrangement of the molecules is still maintained. Furthermore, it is of interest in the molecular superstructure that the chirality of [A1] unit cell is opposite to that of [A2] unit cell.²⁶

D. After Monolayer. After the formation of the ordered monolayer on Au(111), more FePc molecules were deposited with the same experimental conditions. The FePc multilayer of different coverages are fabricated. Due to the smaller sticking coefficient of the molecules on the first monolayer than on the bare Au(111) substrate, more time is generally needed for the deposition of the same amount of molecules. Figure 3(a) shows a large scale STM image of the FePc multilayer at a coverage of ~ 1.3 mL. As seen in the STM image, most of the molecules formed well-ordered islands and only fewer molecules randomly adsorb on the first layer as clusters or individual molecules. It is clear that all the step edges of the molecular islands are straight along the $[\bar{1}2\bar{1}]$ and $[10\bar{1}]$ directions, marked by the arrows, as shown in Figure 3(a). The zigzag pattern from the Au(111) surface reconstruction is observable as a modulation of the multilayer, indicating that the Au(111) surface reconstruction is not destroyed. The FePc multilayer at a coverage of ~ 1.7 mL is shown in Figure 3(b) in which the sizes of the islands are larger than those in Figure 3(a). A comparison between Figure 3(a) and Figure 3(b) makes it clear that the growth of the second layer prefers the layer-by-layer mode in contrast to that of the first monolayer growth, which indicates that the effect

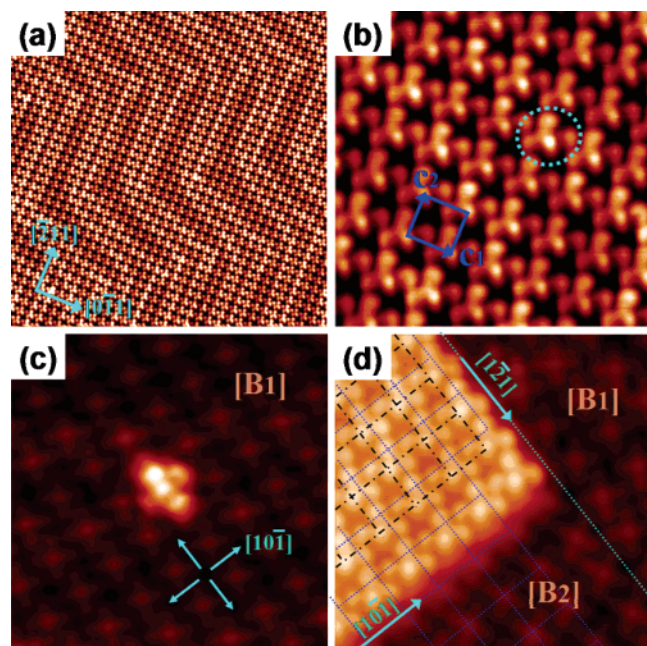


Figure 4. STM images of the second FePc layer (a) and (b) on Au(111). (a) 50 nm \times 50 nm, $V = -2.2$ V, $I = 0.05$ nA; (b) 10 nm \times 10 nm, $V = -2.2$ V, $I = 0.05$ nA. One unit cell and one FePc molecule are marked with a square and a circle, respectively, in (b). (c) STM image (10 nm \times 10 nm, $V = -0.4$ V, $I = 0.05$ nA) of single FePc molecule adsorbing on the first layer. (d) STM image (10 nm \times 10 nm, $V = -0.4$ V, $I = 0.05$ nA) of the first and second FePc layer. The adsorption configuration of FePc molecules on the first layer and the superstructure relation between the first and second layer on Au(111) are shown in (c) and (d), respectively. The color scale extends over a range of 0.12 nm in (a) and (b) and a range of 0.23 in (c) and (d).

of the Au(111) surface reconstruction on the growth of the second layer has decreased remarkably. So it can be concluded that the interaction between the molecules of the second layer and the substrate have been distinctly weakened because of the screening effect of the first layer.

A large scale STM image of the FePc second layer is shown in Figure 4(a), which shows a perfect periodic structure of the second FePc layer. A quadratic periodic structure of the FePc second layer was found in which the molecules are aligned one by one along the $[0\bar{1}1]$ and $[\bar{2}11]$ directions. As shown in Figure 4(b), a square unit cell is marked by blue lines in which the blue arrows (\mathbf{c}_1 , \mathbf{c}_2) represent the unit cell vectors of the molecular superstructure. Analysis of LEED patterns, Fourier transformation of Figure 4(a), and the STM data shown in Figure 4(b) are in good agreement, indicating that the superstructure matrix of the second layer is the same with that of the first layer. The FePc molecules in the second layer exhibit a triangle structure with only three lobes and a central protrusion, marked by a dotted circle in Figure 4(b), indicating a nonplanar adsorption configuration.

To fully comprehend the nonplanar molecular configuration in the second layer, we studied the single FePc molecule adsorbed on the first layer ([B1] domain) shown in Figure 4(c). It can be seen that the molecule is tilted by $\sim 40^\circ$ to the substrate surface plane along the $[10\bar{1}]$ direction with a lobe downward to the substrate and trapped at the central hole of one unit cell in the first layer. The tilted angle of $\sim 40^\circ$ is estimated by a comparison between the sizes of the roughly flat-lying molecule and the molecule in Figure 4(c). So the downward lobe appears dark, while the other three lobes appear bright in Figure 4(c). As to the molecules within the second layer, the downward lobe is fully unobservable, so the molecule is recognized as a triangle

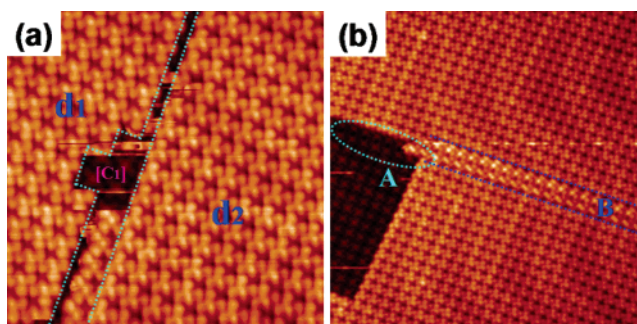


Figure 5. (a) STM image (20 nm \times 20 nm, $V = -2.2$ V, $I = 0.05$ nA) of two domains in the second layer. (b) STM image (40 nm \times 40 nm, $V = -2.2$ V, $I = 0.05$ nA), showing the relation between the defects of the first layer and that of the second layer on Au(111). The color scale extends over a range of 0.35 nm in both (a) and (b).

structure with only three lobes and a central protrusion in Figure 4(b). Because of the quadratic ordering of the first layer, the molecule can be tilted along four directions equivalently, marked by the arrows in Figure 4(c). Figure 4(d) shows both the first and second layers. The boundary between the [B1] and [B2] domains in the first layer is marked by dashed line. The island of the second layer is on the top of the [B2] domain with straight step edges along the $[10\bar{1}]$ and $[\bar{1}21]$ directions of the Au(111) substrate. The molecule at the corner of the second layer represents the similar configuration with that of the single molecule in Figure 4(c). And there is a slight difference between them, which is possibly due to the interactions between the molecules of the second layer. The intersections of the dashed square lattice in the image represent the iron atoms of the FePc molecules in the [B2] domain, and that of the dashdotted square lattice for the iron atoms of the FePc molecules in the second layer, which clearly indicates that the superstructure of the second layer is identical to that of the first layer and the central metal atoms of FePc in the second layer do not stay exactly on the right top of Fe atoms in the first layer. The identical superstructure of the two layers is the result of the adsorption configuration of the molecule.

As shown in Figure 4(c), each FePc molecule has four tilted directions on the single orientation-domain of the first layer. In Figure 5(a), there are two different domains (\mathbf{d}_1 and \mathbf{d}_2) of the second layer on the [C1] domain of the first layer. It is apparent that the two domains prefer the identical quadric superstructure, but opposite tilted directions. The domain boundary area between the two domains is marked with dashed lines, in which an array of molecules preferring another adsorption configuration is observed. And near the boundary area, the highly ordered arrangements of two domains are maintained.

Understanding and controlling the defect formation during the epitaxial growth process are significant to improve the performance of organic devices. As shown in Figure 5(b), the line defect in the first layer marked by dashed circle (A) influences the adsorption configurations of the molecules on it. So the molecules on the line defect show special adsorption configurations different from the normal one, forming the line defect (B) in the second layer. Apparently the defects in the initial layer can induce new defects in the second layer, then the third layer. Therefore, the quality of the initial molecular layers has a very important effect on the further growth of organic films.

The electronic properties of the MPc–substrate interfaces are dependent on the structures of the initial MPc layers, especially the molecular ordering and configuration within the first and second layers. Tada et al. investigated epitaxial trilayer CoPc

films on Au(111) surface to determine the arrangements and orientations of molecules.³⁰ Their results revealed that CoPc molecules of the first layer stay with their molecular planes parallel to the substrate surface, whereas those in the second layer are tilted by $\sim 3^\circ$ to the substrate surface and the central Co atoms of CoPc in the second layer stay exactly on top of the Co atoms in the first layer with no lateral displacement between the Co atoms of two layers.

Conclusions

We report on LT-STM investigation of FePc molecules adsorbed on Au(111) surface in the whole growth process from the initial adsorption to the multilayer growth. The FePc molecules prefer to separately adsorb on the fcc and the hcp regions at the submonolayer regime, indicating that the adsorption is greatly affected by the molecule–substrate interaction. At the monolayer regime, the molecules can form a close-packed ordered structure. When the FePc goes further to the second layer, the unit cell of the formed molecular structure shifts compared with the unit cell of the first layer. Comparison of the growth behavior between FePc and CoPc also is made to understand the growth difference within the family of the Pc molecules.

Acknowledgment. This project is supported partially by the Natural Science Foundation of China (NSFC) (Grant Nos. 60276041, 90406022, 90201036).

References and Notes

- (1) Crone, B.; Dodabalapur, A.; Lin, Y. Y.; Filas, R. W.; Bao, Z.; LaDuca, A.; Sarpeshkar, R.; Katz, H. E.; Li, W. *Nature (London)* **2000**, *403*, 521.
- (2) Dimitrakopoulos, C. D.; Malenfant, P. R. L. *Adv. Mater.* **2002**, *14*, 99.
- (3) Witte, G.; Wöll, C. *J. Mater. Res.* **2004**, *19*, 1889.
- (4) Horowitz, G. *J. Mater. Res.* **2004**, *19*, 1946.
- (5) Gao, H.-J.; Sohlberg, K.; Xue, Z. Q.; Chen, H. Y.; Hou, S. M.; Ma, L. P.; Fang, X. W.; Pang, S. J.; Pennycook, S. J. *Phys. Rev. Lett.* **2000**, *84*, 1780.
- (6) Barlow, S. M.; Raval, R. *Surf. Sci. Rep.* **2003**, *50*, 201.
- (7) Eremitchenko, M.; Schaefer, J. A.; Tautz, F. S. *Nature (London)* **2003**, *425*, 602.
- (8) Forrest, S. R. *Chem. Rev.* **1997**, *97*, 1793.
- (9) Mannsfeld, S. C. B.; Fritz, T. *Phys. Rev. B.* **2005**, *71*, 235405.
- (10) Theobald, J. A.; Oxtoby, N. S.; Phillips, M. A.; Champness, N. R.; Beton, P. H. *Nature (London)* **2003**, *424*, 1029.
- (11) Böhringer, M.; Morgenstern, K.; Schneider, W. D.; Berndt, R.; Mauri, F.; De Vita, A.; Car, R. *Phys. Rev. Lett.* **1999**, *83*, 324.
- (12) Barth, J. V.; Weckesser, J.; Cai, C.; Günter, P.; Bürgi, L.; Jeandupeux, O.; Kern, K. *Angew. Chem., Int. Ed.* **2000**, *39*, 120.
- (13) Yan, H. J.; Lu, J.; Wan, L. J.; Bai, C. L. *J. Phys. Chem. B.* **2004**, *108*, 11251–11255.
- (14) Scudiero, L.; Hipps, K. W.; Barlow, D. E. *J. Phys. Chem. B.* **2003**, *107*, 2903–2909.
- (15) Han, P.; Mantoosh, B. A.; Sykes, E. C. H.; Donhauser, Z. J.; Weiss, P. S. *J. Am. Chem. Soc.* **2004**, *126*, 10787–10793.
- (16) Lukas, S.; Witte, G.; Wöll, Ch. *Phys. Rev. Lett.* **2002**, *88*, 028301.
- (17) Gao, L.; Deng, Z. T.; Ji, W.; Lin, X.; Cheng, Z. H.; He, X. B.; Shi, D. X.; Gao, H.-J. *Phys. Rev. B.* **2006**, *73*, 075424.
- (18) Wang, Y. L.; Ji, W.; Shi, D. X.; Du, S. X.; Seidel, C.; Ma, Y. G.; Gao, H.-J.; Chi, L. F.; Fuchs, H. *Phys. Rev. B.* **2004**, *69*, 075408.
- (19) Seidel, C.; Poppensieker, J.; Fuchs, H. *Surf. Sci.* **1998**, *408*, 223.
- (20) Joachim, C.; Gimzewski, J. K.; Aviram, A. *Nature (London)* **2000**, *408*, 541.
- (21) Craciun, M. F.; Rogge, S.; Morpurgo, A. F. *J. Am. Chem. Soc.* **2005**, *127*, 12210–12211.
- (22) Papageorgiou, N.; Salomon, E.; Angot, T.; Layet, J. M.; Giovannelli, L.; Lay, G. L. *Prog. Surf. Sci.* **2004**, *77*, 139–170.
- (23) Lu, X.; Hipps, K. W.; Wang, X. D.; Mazur, U. *J. Am. Chem. Soc.* **1996**, *118*, 7197.
- (24) Hipps, K. W.; Lu, X.; Wang, X. D.; Mazur, U. *J. Phys. Chem.* **1996**, *100*, 11207.
- (25) Lu, X.; Hipps, K. W. *J. Phys. Chem. B.* **1997**, *101*, 5391.
- (26) Barlow, D. E.; Hipps, K. W. *J. Phys. Chem. B.* **2000**, *104*, 5993.
- (27) Yoshimoto, S.; Tada, A.; Suto, K.; Itaya, K. *J. Phys. Chem. B.* **2003**, *107*, 5836–5843.
- (28) Suto, K.; Yoshimoto, S.; Itaya, K. *J. Am. Chem. Soc.* **2003**, *125*, 14976–14977.
- (29) Yoshimoto, S.; Tsutsumi, E.; Suto, K.; Honda, Y.; Itaya, K. *Chem. Phys.* **2005**, *319*, 147–158.
- (30) Takada, M.; Tada, H. *Chem. Phys. Lett.* **2004**, *392*, 265–269.
- (31) Barlow, D.; Scudiero, L.; Hipps, K. W. *Ultramicroscopy* **2003**, *97*, 47–53.
- (32) McGhie, A. R.; Garito, A. F.; Heeger, A. J. *J. Cryst. Growth* **1974**, *22*, 295.
- (33) Ekavli, I.; Wahlström, E.; Claesson, D.; Olin, H.; Olsson, E. *Meas. Sci. Technol.* **1999**, *10*, 11–18.
- (34) Barth, J. V.; Brune, H.; Ertl, G.; Behm, R. *J. Phys. Rev. B.* **1990**, *42*, 9307.
- (35) Chizhov, I.; Scoles, G.; Kahn, A. *Langmuir* **2000**, *16*, 4358–4361.
- (36) Okudaira, K. K.; Hasegawa, S.; Ishii, H.; Seki, K.; Harada, Y.; Ueno, N. *J. Appl. Phys.* **1999**, *85*, 6453–6461.